

High-speed cylindrical grinding of SiC: The process characteristics and surface integrity

Jiaming Ni*, Beizhi Li and Jingzhu Pang

Faculty of Mechanical Engineering, Donghua University, 2999 Renming Road (N), Shanghai 201620, China

In recent years SiC has emerged in industrial applications. However, due to its unique thermal and mechanical properties, economical machining always meets obstacles. In this study, high-speed grinding in conjunction with a high workpiece speed by a diamond grinding wheel is proposed as a solution. A rotating-4-component-dynamometer has been employed for the force measurements, followed by a series of tests on the surface quality including surface roughness, scanning electron microscope observations and residual stress analysis. It has been found that the combination of the elevated grinding wheel speed and the higher workpiece speed can lead to low grinding forces and thermal energy at almost all levels of the material removal rate in this study. Besides, the grinding-induced damage layer will be eliminated and the surface quality can be improved. With an elevated wheel speed, a brittle-ductile transition can be found based on the observation of the ground surface and the orientation of the surface roughness and the residual stresses. In view of the grinding energy analysis and surface quality tests, it can be concluded that high-speed grinding is an effective solution for the high quality and high efficiency cylindrical grinding of SiC.

Key words: High-speed grinding, Ceramic, Surface integrity, SiC.

Introduction

Silicon carbide is a member of a group of materials usually termed the non-oxides, in which silicon carbide is the most widely used for its notable hardness, very high melting-point and other extremely useful properties [1]. The main application areas for silicon carbide ceramics are, for example, mirrors, pumps and valves, diesel engine exhausts and gas-turbine engine components [2, 3]. Although advances have been made in the near-net shape technology, high dimensional accuracy and good surface integrity are frequently required in structural ceramic components [4, 5]. So grinding with diamond wheels is still the method of choice for the machining of these structural ceramics [5-8].

In the past decades, high-speed grinding has been developed as a finishing process in order to avoid the grinding-induced damage layer on the ceramics [9, 10]. However, these investigations were limited to silicon nitride [11-13], and zirconia [13, 14]. In recent years silicon carbide has also emerged as a structural material whose applications are very limited in the literature. The high-speed grinding of SiC has been reported by Ramesh et al. [15] and Huang and Malkin [10], but both studies were conducted on the surface grinding with a relatively low workpiece speed in comparison with the present investigation. What is more, few publications are available on the residual stresses and

the depth profile of the ground SiC surface layer.

So in this paper, a series of tests were conducted on a cylindrical-grinding machine to investigate the relationship between the grinding characteristics and the grinding-induced damage of SiC. Besides, the combination of elevated wheel speed and higher workpiece speed will be expected to lead to a better surface quality and a higher material removal rate. The residual stresses and their depth profiles in cooperation with the microscopic observations on the surface and subsurface will provide a complete understanding of the efficient and high quality grinding of SiC.

Practical Investigation

Grinding experiments were performed on the MGKS 1332/H CNC cylindrical grinding machine in Shanghai Machine Tool Works Ltd. A ceramic bond diamond-grinding wheel, with an average grit size of 91 μm was used (with a diamond concentration of 150%). The wheel has a diameter of 400 mm and a width of 15 mm. The work material used for this investigation was SiC, whose properties are given in Table 1. The specimens have the diameter of $\Phi 100$ mm with the length of 60 mm. The grinding conditions used for this work are listed in Table 2.

The normal and tangential grinding forces, F_n and F_t , were measured using a rotating-4-component-dynamometer including a piezo-electric force transducer from Kistler (9123C). Force signals were recorded by a personal computer via a data acquisition system (PCIM-DAS1602/16), and then filtered by DIAdem software with a cut-off frequency of 3000 Hz.

*Corresponding author:
Tel : +86-021-6779-2581
Fax: +86-021-6779-2581
E-mail: njm126@mail.dhu.edu.cn

Table 1. Mechanical properties of SiC used in the experiments

Material properties							
Grain Size	Density	Bending strength	Hardness (HV10)	Fracture toughness	Modulus of elasticity	Poisson ratio	
d_g [μm]	ρ [g/cm^3]	σ_{3b} [MPa]	Hv [GPa]	K_{IC} [$\text{MPa}\cdot\text{m}^{1/2}$]	E [GPa]	r [-]	
SiC	10	3.22	490	22 - 25	3 - 4	410	0.16

Table 2. Grinding conditions

Grinding wheel velocity	Workpiece speed	Grinding depth	Material removal rate
v_s [m/s]	v_w [$\text{m}\cdot\text{minute}^{-1}$]	a_e [μm]	Q'_w [$\text{mm}^3/\text{mm}\cdot\text{s}$]
20 - 80	4.8	13	1.00
20 - 80	4 - 16 ($q = v_s/v_w = 250$)	3.8 - 15	1.00
20 - 80	4 - 16 ($q = v_s/v_w = 250$)	17	1.36 - 5.44

The ground surfaces cleaned with acetone were examined by an optical microscope equipped with a digital imaging system (KH-7700 Digital Microscope System). The surface roughness values were measured using a 3D optical profilometer (NPFLEX). A bonded interface sectioning technique [16] was used to examine the grinding-induced subsurface damage. Two specimens polished with 1 μm diamond paste were bonded face-to-face with a cyanoacrylate-based adhesive. A clamping pressure was applied to push the two specimens tightly together, leaving a thin layer of glue approximately 1 μm thick. Then the grinding was conducted on the cylindrical surface. With a scanning electron microscope (SEM), the residual damage can be observed on the polished surfaces, especially for the brittle fracture and cracks induced in the grinding process.

Results and Discussion

Mechanical load aspect

Grinding damage in brittle materials originating from the mechanical load is mainly due to the normal grinding force, F_n , while the tangential grinding force, F_t , will induce a thermal load [17, 18]. The normal force component can produce various crack systems. For SiC, grinding conducted at $v_s = 80$ m/s exerted only one fourth of the normal and tangential grinding forces obtained at $v_s = 20$ m/s shown in Fig. 1 (a). Furthermore, keeping the speed ratio $q = 250$, the specific normal and tangential grinding forces scaled relatively steady, at about 25 N/mm and 8 N/mm, respectively, almost regardless of the specific material removal rate (Fig. 1 (b)).

Quantitatively the parameter $h_{cu\ max}$, defines as the maximum depth of cut taken by an individual cutting point on the wheel surface, and characterizes the depth of penetration of the abrasive grain into the workpiece

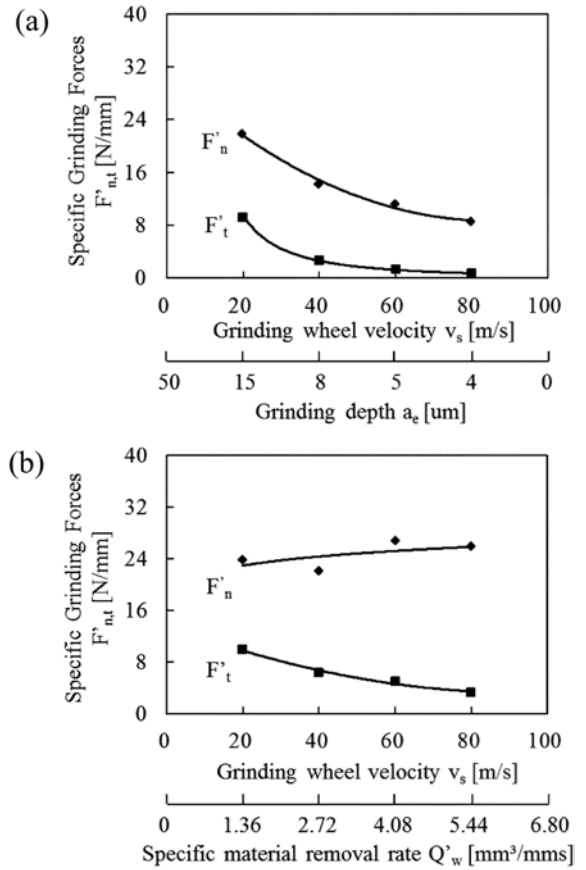


Fig. 1. The effect of the grinding wheel velocity on the specific grinding forces and force ratio under $v_s/v_w = 250$, (a) $Q'_w = 1$ $\text{mm}^3/\text{mm}\cdot\text{s}$ and (b) $a_e = 0.017$ mm.

when it engaged in cutting [19]. Approximating the undeformed chip cross-section as triangular, $h_{cu\ max}$ can be written for cylindrical grinding as:

$$h_{cu\ max} \approx \left(\frac{3}{C_{stat} \cdot \tan\theta} \right)^{\frac{1}{2}} \cdot \left(\frac{v_w}{v_s} \right)^{\frac{1}{2}} \cdot \left(\frac{a_e}{d_{eq}} \right)^{\frac{1}{4}}, \quad (1)$$

where C_{stat} is the static cutting edge density, θ is the semi-induced angle for the undeformed chip cross-section and d_{eq} is the equivalent diameter of the grinding wheel. Smaller values of $h_{cu\ max}$ are expected to give a longer wheel life, lower grinding forces and temperature, and better ground surface integrity [9, 10, 20]. For the 91 μm diamond grinding wheel applied in the current study, $C_{stat} = 30$ mm^{-2} based on the SEM observations and $\theta = 60^\circ$ are considered [14]. Based on the calculation of the maximum undeformed chip thickness, it can be seen, that the $h_{cu\ max}$ value at a high speed of $v_s = 80$ m/s is only 70% of that at the conventional speed of 20 m/s. While, also keeping $q = 250$ and $a_e = 17$ μm , an increase of the removal rate does not change the chip thickness according to the Eq. (1).

In Fig. 2, the specific grinding forces and force ratio are plotted against the $h_{cu\ max}$ values. In the test range, the specific normal grinding force keeps relatively steady, at about 24 N/mm, while the specific tangential

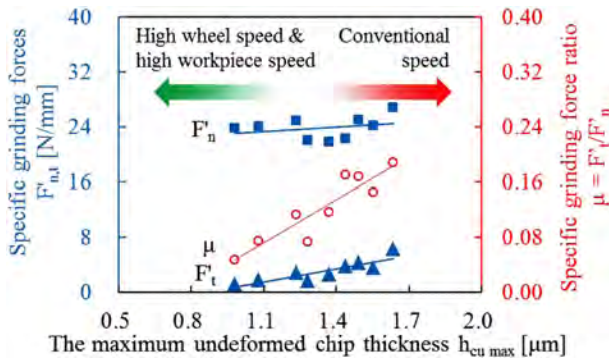


Fig. 2. The $h_{cu\ max}$ value vs. the specific grinding forces and specific grinding force ratio.

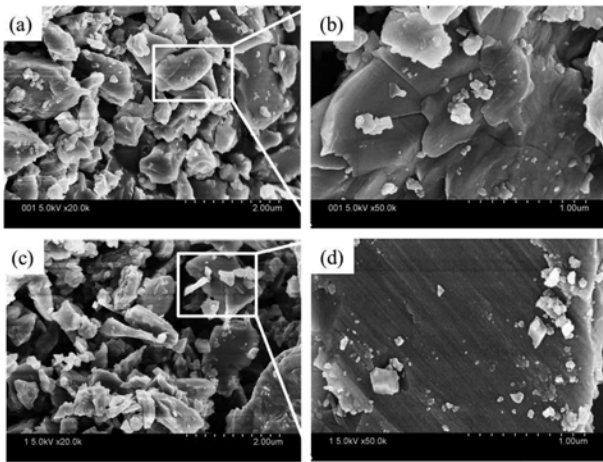


Fig. 3. SEM examination of SiC grinding chips under $v_w = 4.8$ m/min and $a_c = 13$ μ m, (a, b) at $v_s = 20$ m/s and (c, d) at $v_s = 80$ m/s.

grinding force increases from 1.12 N/mm to 6.30 N/mm with the increment of $h_{cu\ max}$. An interesting phenomenon is that a smaller $h_{cu\ max}$ value gives a much smaller force ratio about 0.06 as seen in Fig. 2. Although the machining of SiC is mainly in the form of a brittle removal mode, the abrasive-workpiece interactions can still be generally modeled as sliding, plowing, cutting and chipping [21]. Given a constant material removal rate, the combination of an elevated wheel speed and higher workpiece speed will lead to a decline of the maximum undeformed chip thickness, according to Eq. (1). Also a thinner chip thickness will further decrease the contact area between the grinding chip and the rake face of the abrasive grit, leading to a decline of the friction. Therefore the high-speed grinding has the potential to reduce the grinding forces and the friction between the abrasive grit and the ceramic.

SEM observations of grinding debris, ground surface and subsurface

Because of the great brittleness and low plasticity, the grinding of ceramic SiC will easily induce microcracks on the ground surfaces and in the sub-surface layers. Microscopic observations of the grinding debris and ground surfaces can provide direct evidence about the

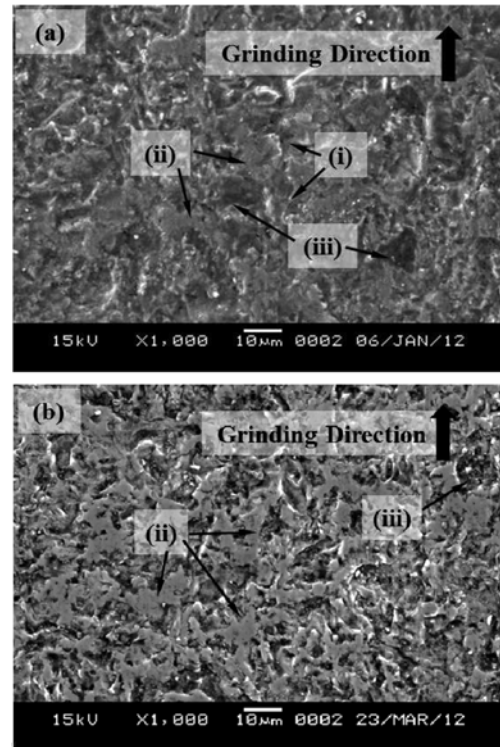


Fig. 4. Ground surface characteristics of SiC under $v_w = 4.8$ m/min and $a_c = 13$ μ m, (a) $v_s = 20$ m/s, (b) $v_s = 80$ m/s, ((i) indicates the brittle fractures, (ii) indicates the smeared area by plastic deformation and (iii) indicates the grains dislodgement).

prevailing grinding mechanisms. Grinding debris for SEM observation was collected from the spark stream, dried at room temperature, and then sputter coated with gold. SEM micrographs of grinding debris collected for SiC ground with the 91 μ m diamond grinding wheel are shown in Fig. 3. The debris consists mostly of relatively large cubic-like particles (Fig. 3 (a)) with a diameter of 1 - 2 μ m which appear to be fractured from the workpiece by lateral cracking, and much finer particles (Fig. 3 (b, d)) which are generated by crushing. The plate-like particles typically have grinding striations on one side as seen in Fig. 3 (d). The striations may have been generated either immediately before the particle fractured from the workpiece or during the preceding grinding pass. In Fig. 3 (a, b) crack breaks along the grain boundary can be seen. However, in Fig. 3 (c, d) the high impact by the elevated wheel speed broke the grains and changed chip profile in comparison with that at the low wheel speed. These and numerous other SEM observations indicate that grinding debris is generated mainly by crack nucleation, crack propagation and brittle fracture. Similar observations have been reported for other brittle workpiece materials [22-24].

The SEM images of the ground surfaces (Fig. 4) show that although ductile and brittle removal modes can occur, a third removal mode that consists of the formation of microcracks along the grain boundaries is more predominant at most conventional grinding speeds (Fig. 4 (a)) applied to polycrystalline SiC [25].

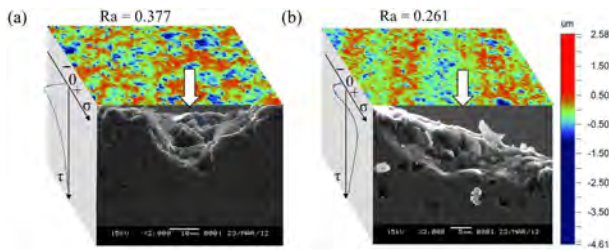


Fig. 5. Ground surface morphology and subsurface damage of SiC under $v_w = 4.8$ m/min and $a_c = 13$ μm , (a) $v_s = 20$ m/s, (b) $v_s = 80$ m/s; (arrows indicate the ground surface).

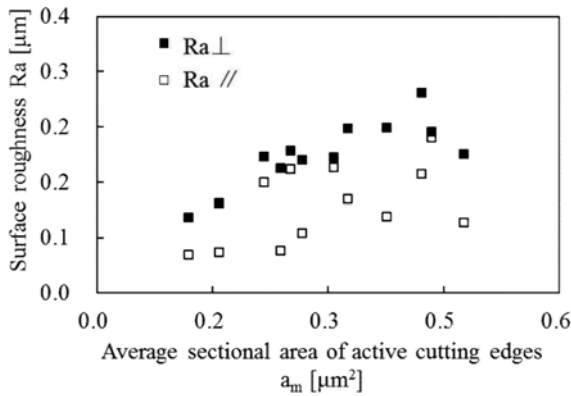


Fig. 6. Surface roughness as a function of average sectional area of active cutting edges.

The energy for the grain boundary crack is normally lower than that for the fracture of the grain [1]. Hence grain boundary cracks are preferred in rough grinding to reduce the grinding energy, while the fracture of the grains is widely used for the finish grinding to generate a smooth surface. For SiC, the surface texture had improved considerably at a high wheel speed (Fig. 4 (b)). The size of chipping was reduced but the mechanism of material removal was little changed. Ground silicon carbide showed a typical grinding structure, with large ground smeared areas observable on the ground surface. No large grain pulled out defects can be seen under the $v_s = 80$ m/s, but most of the chip removal of SiC was still due to brittle fracture. These may indicate the presence of a brittle fracture during chipping.

Subsurface damage of the ground specimens, which were prepared using the bonded interface sectioning technique, was examined using SEM. Two types of subsurface damage, chipping and cracking, induced by grinding were clearly observed [25]. The damaged layer right underneath the machined surface is seen to be generated via chipping, and the chipping layer is seen to be induced mainly by grain dislodgement as shown in Fig. 5. At $v_s = 20$ m/s, a large grain dislodgement induced by grain-boundary microcracks could be seen right underneath the machined surface. However, at an elevated wheel speed of 80 m/s, the chipped layer appears to be uniform along the subsurface and the subsurface damage thickness is smaller in comparison with that at $v_s = 20$ m/s. This could be due to fact that as

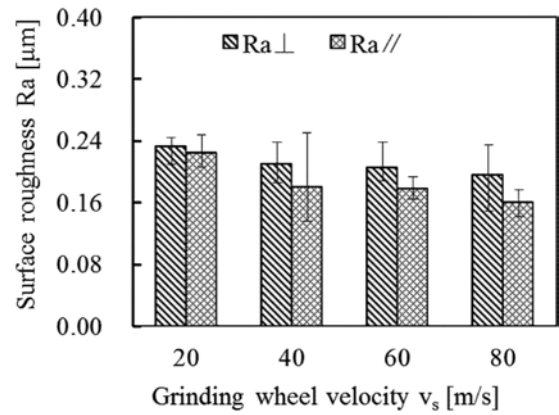


Fig. 7. Surface roughness as a function of grinding wheel velocity under $v_s/v_w = 250$ and $Q_w^3 = 1$ $\text{mm}^3/\text{mm}\cdot\text{s}$.

Table 3. ANOVA for surface roughness data

Source of variation	Sum of squares	Degrees of freedom	Mean square	F	Prob > F	Remark
Wheel speed	0.00905	3	0.00302	3.71	0.0425	Significant at 95% confidence level
Error	0.00974	12	0.00081			
Total	0.01879	15				

the grinding wheel velocity was increased, the local contact force and the number of contacting diamond particles would increase, leading to a smaller damage layer in the subsurface.

Surface roughness and morphology

The topography of a ground surface can serve as an indicator of the predominant mechanisms of material removal. In metal grinding, the grits produce grooves by their cutting and ploughing action. With many brittle ceramics, material is removed via microfracture, thus leaving an irregular surface with isotropic roughness. To determine the amount of plastic deformation, roughness measurements are performed in the grinding direction and perpendicular thereto. Fig. 6 shows the surface roughness of SiC over the wide range of grinding conditions. Although the SiC is brittle on a microscopic scale, the roughness value perpendicular to the grinding direction is higher than that parallel thereto indicating that a considerable amount of plastic deformations on the ground surface resulting from ductile material behavior in grinding, which was also observed by Inasaki [26]. In particular a smaller average sectional area of active cutting edges can provide a better surface roughness as shown in Fig. 6.

The variation of surface roughness with grinding wheel velocity is shown in Fig. 7. Each data point is the average of five measurements and the error bars indicate the maximum and minimum values of surface roughness measured. The analysis-of-variance (ANOVA) technique was used in order to conduct a statistical

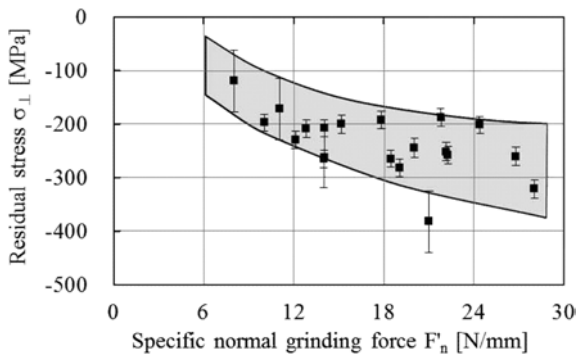


Fig. 8. Surface residual stress σ_{\perp} vs. specific normal grinding force F'_n .

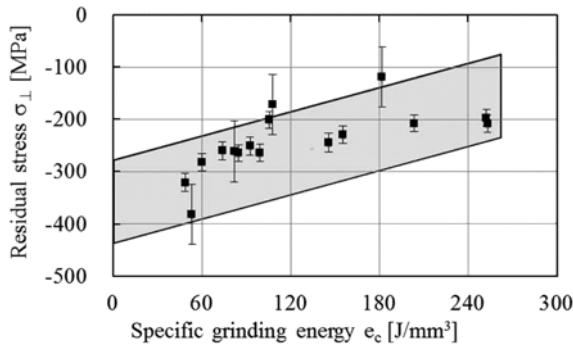


Fig. 9. Surface residual stress σ_{\perp} vs. specific grinding energy e_c .

analysis. The results of ANOVA for surface roughness are summarized in Table 3. It could be seen from the table that the probability larger than F is only 0.0425. That is, the grinding wheel velocity significantly affected the surface roughness.

In order to verify above analysis, the ground surfaces were also observed in more detail by the 3D optical profiling microscope and the images are shown in Fig. 5. The profile images show that under a same material removal rate, a brittle-ductile transition can be seen during grinding of SiC when the wheel speed increased from 20 m/s to 80 m/s.

The properties, orientation and depth profile of residual stress

The residual stress is a result of the thermo-mechanical load during the grinding process. In grinding, mechanical loading produces a compressive stress while a tensile stress is attributed to thermal influence [27]. Fig. 8 and Fig. 9 plot the residual stresses found in ground specimens of SiC vs. F'_n and the specific grinding energy, e_c . It is found that residual stress on the ground surface is compressive in all cases. Combined with the large smeared area on the ground surface of SiC in the SEM images (Fig. 4) and the large degree of visible plastic deformation observed in the 3D optical profiling images (Fig. 5), this result suggests mechanical loading as the principal cause for residual stress.

The influence of high grinding temperatures on

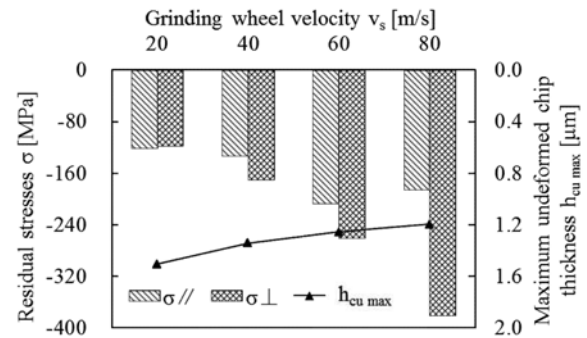


Fig. 10. The influence of grinding wheel velocity on the residual stress orientation.

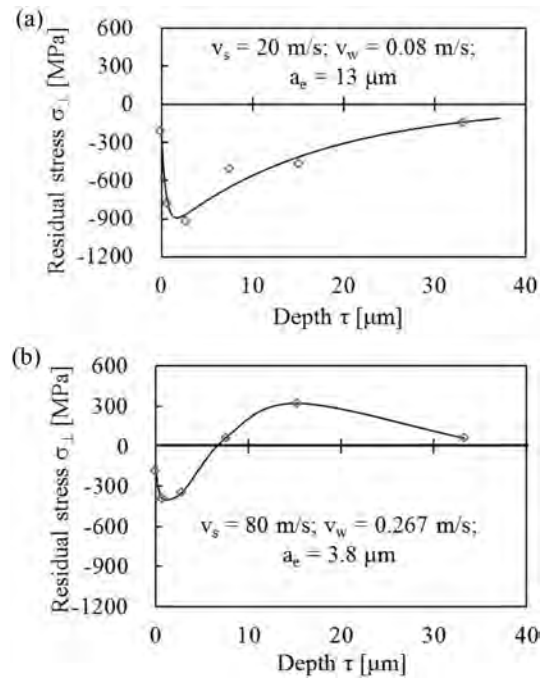


Fig. 11. Residual stress distribution for the grinding process under material removal rate of $1 \text{ mm}^3/\text{mm} \cdot \text{s}$.

surface integrity is equally important, as Fig. 9 shows. With the combination of elevated wheel speed and higher workpiece speed, grinding operations with a low specific normal force are also associated with a low grinding energy (Fig. 1), regardless of the material removal rate. For SiC grinding, the brittle fracture energy [10] and the specific kinetic energy of the chips [28] are so small that they could be neglected. Therefore, most of the grinding energy must be expended by ductile flow, even though material removal is mainly by brittle fracture [10]. The friction between the abrasive grit and SiC can lead to a high thermal energy, which is reflected by the elevated grinding temperature. Therefore this indicates that a grinding condition with a low grinding temperature rise, can lead to a higher compressive residual stress as shown in Fig. 9.

For the description of correct states of residual stress in SiC it is necessary to analyze the orientations of the main stress directions apart from the absolute values.

From metallic materials it is known that non-directional processes like thermal effects produce no preferred orientation of the residual stress. In contrast to this, processes with a given effective direction, for example the cutting action in grinding, show a distinctive dependence of grinding direction [29-31]. As is shown in Fig. 10, given that the material removal rate is constant, an elevated grinding wheel speed will lead to a smaller $h_{cu\ max}$ value. When the $h_{cu\ max}$ of individual abrasive grit is less than a critical-depth-of-penetration that causes brittle fracture in a material, then the grinding will occur in the ductile regime [32]. So in Fig. 10 it can be seen that with the decline of the chip thickness, the orientation becomes more dominant. This indicates that the elevated wheel speed and higher workpiece speed can lead to a brittle-ductile transition.

Unlike metals, the structural ceramics cannot be electro-chemically polished to remove the material layer by layer. Therefore, with the aid of a single exposure technique $d\text{-sin}^2(\Psi)$ method as mentioned in the appendix, the depth profile of the residual stress could be determined. As is shown in Fig. 11 (a, b), the maximum stress is located a certain distance beneath the ground surface. For ceramics, under excessive mechanical loading subsurface cracks may develop and locally relieve the level of the compressive stress, which is the reason for the small value of the residual stress on the top surface. With an increase of the grinding wheel speed and the reduction of the value of $h_{cu\ max}$, the absolute value of the residual stress becomes smaller but the incremental engagement between the grit and the workpiece will induce more friction and result in a tensile stress beneath the top surface as shown in Fig. 11 (b).

Conclusions

In the present study, high-speed cylindrical grinding was conducted for silicon carbide to investigate the grinding characteristics and surface integrity, while a ceramic bonded diamond wheel was used as the grinding tool. It was found that:

- (1) The application of a rotating-4-component-dynamometer is approved to be an efficient solution for the force measurement during cylindrical grinding of SiC.
- (2) The combination of the elevated grinding wheel speed and the higher workpiece speed can lead to low grinding forces and thermal energy at almost all levels of material removal rate in this study.
- (3) The high speed grinding in cooperation with high workpiece speed can produce a desired residual stress status and its depth profile. The mechanical load and the grinding energy can also be reduced by the application of a faster workpiece speed. The coupling mechanism of the thermo and mechanical load on the surface will finally determine the residual stress distribution.

- (4) A brittle-ductile transition can be observed during grinding of SiC when the wheel speed increased from 20 m/s to 80 m/s, indicating that high-speed grinding is a useful solution for the high efficiency and high quality grinding of structural ceramics.

Acknowledgement

This work is a part of the National Basic Research Program of China (2009CB724403) and the National High Technology Research and Development Program of China (2012AA041309). The authors wish to record their gratitude to their generous supports.

Appendix

A so called single exposure technique $d\text{-sin}^2(\Psi)$ method has been employed for the analysis of the residual stresses in the subsurface. Modern goniometers enable a diffractometer to operate at very small incident angles, e.g. less than 1° , with high accuracy. In this technique, a small incidence angle of the X-ray beam interacts with larger area of the material surface [33]. The actual path length of the X-rays is deviated due to the effect of the refraction at very small incident angles. The effective penetration depth, τ is calculated by:

$$\tau = \frac{1}{\mu \{ 1/[\cos^{-1}((\cos\alpha)/n)] + 1/[\cos^{-1}((\cos\gamma)/n)] \}}, \quad (2)$$

where μ is the linear absorption coefficient of X-rays in the material, α is the incident angle, γ is the departure angle and n is the refraction index. In this paper, the refraction index $n = 0.99998966$. The mass absorption coefficient of a substance containing more than one element can be determined from the following expression [34]:

$$(\mu/\rho)_{SiC} = w_{Si}(\mu/\rho)_{Si} + w_C(\mu/\rho)_C, \quad (3)$$

where ρ is the density of the element, w_{Si} and w_C are the weight fractions of elements Si and C in SiC respectively, $(\mu/\rho)_{SiC}$, $(\mu/\rho)_{Si}$, $(\mu/\rho)_C$ are the mass absorption coefficients of SiC, Si and C, respectively. By using Eq. (3) with the data listed in Table 4 and Table 1, the linear absorption coefficient of Cu K_α radiation in SiC is determined to be 151.76 cm^{-1} .

Table 4. Data used for the calculation of linear absorption coefficient of Cu K_α radiation in SiC

Element	Atomic Weight	Density	Mass absorption coefficient
		ρ [g/cc]	μ/ρ [cm^2/g]
Si	28.086	2.33	65.32
C	12.011	2.26	4.6

References

1. F. Riley, in *Structural Ceramics: Fundamentals and Case Studies*, Cambridge University Press (2009).
2. H. Kasuga, H. Ohmori, T. Mishima, Y. Watanabe and W. Lin, *J. Ceram. Process. Res.* 10 [3] (2009) 351-354.
3. J. Briggs, in *Engineering Ceramics in Europe and the USA*, Enceram Press (2007).
4. I.D. Marinescu, H.K. Tönshoff and I. Inasaki, in *Handbook of Ceramics Grinding & Polishing*, William Andrew Press (1999).
5. S. Malkin and T.W. Hwang, *CIRP Ann-Manuf. Techn.* 5 [2] (1996) 569-580.
6. I.D. Marinescu, in *Handbook of Advanced Ceramics Machining*, CRC Press (2007).
7. K. Kitajima, G.Q. Cai, N. Kurnagai, Y. Tanaka and H.W. Zheng, *CIRP Ann-Manuf. Techn.* 41 [1] (1992) 367-371.
8. B. Zhang and T.D. Howes, *CIRP Ann-Manuf. Techn.* 43 [1] (1994) 305-308.
9. F. Klocke, E. Brinksmeier, C. Evans, T. Howes, I. Inasaki, E. Minke, et al., *CIRP Ann-Manuf. Techn.* 46 [2] (1997) 715-724.
10. T.W. Hwang and S. Malkin, *J. Manuf. Sci. E-T ASME* 121 [4] (1999) 623-631.
11. J.A. Kovach, S. Srinivasan, P.J. Blau, B. Bandyopadhyay, S. Malkin and K. Ziegler, in *Proceedings of the Fifth International Grinding Conference*, SME Technical Paper MR93-M352 (1993).
12. J.A. Kovach, M.A. Laurich, S. Malkin and B. Zhu, in *Proceedings of the Annual Automotive Technology Development Contractors, Coordination Meeting*, Dearborn, Michigan (1994).
13. A.J. Shin, S.B. McSpadden, T.O. Morris, M.B. Grant and T.M. Yonushonis, *Mach. Sci. Technol.* 4 [1] (2000) 43-58.
14. H. Huang and Y.C. Liu, *Int. J. Mach. Tool Manu.* 43 [8] (2003) 811-823.
15. K. Ramesh, S.H. Yeo, S. Gowri and L. Zhou, *Int. J. Adv. Manuf. Tech.* 17 [2] (2001) 87-92.
16. H.H.K. Xu and S. Jahanmir, *J. Am. Ceram. Soc.* 77 [5] (1994) 1388-1390.
17. D.B. Marshall, A.G. Evans, B.T. Kuri Yakub, J.W. Tien and G.S. Kino, *Proc. R. Soc. Lond.* 385 [1789] (1983) 461-475.
18. B.R. Lawn and A.G. Evans, *J. Mater. Sci.* 12 [11] (1977) 2195-2199.
19. F. Klocke, in *Manufacturing Processes 2: Grinding, Honing, Lapping*, Springer-Verlag Berlin Heidelberg (2009).
20. S. Malkin, in *Grinding Technology: Theory and application of machining with abrasives*, Ellis Horwood Press (1989).
21. J. Kajomchaiyakul, *Abrasive Machining of Ceramics: Assessment of Near-Surface Characteristics in High Speed Grinding* [D]. University of Connecticut (2000).
22. J.E. Mayer and G. P. Fang, *NIST Spec. Publ.* 205 [22] (1993) 847.
23. A. Imanaka, S. Fujino and S. Maneta, *NBS Special Pub.* 348 (1972) 37.
24. M. Huerta and S. Malkin, *J. Manuf. Sci. E-T ASME* 98 [2] (1976) 459-467.
25. S. Agarwal and P.V. Rao, *Int. J. Mach. Tool Manu.* 48 [6] (2007) 698-710.
26. I. Inasaki, *CIRP Ann-Manuf. Techn.* 36 [2] (1987) 463-471.
27. E. Brinksmeier, *Prozeß- und Werkstückqualität in der Feinbearbeitung* [D]. Universität Hannover (1991).
28. C. Zeppenfeld, *Schnellhubschleifen von γ -Titanaluminiden* [D]. RWTH Aachen Universität (2005).
29. W. Pfeiffer and T. Hollstein, *J. Eur. Ceram. Soc.* 17 [2-3] (1997) 487-494.
30. E. Brinksmeier and T. Wilke, in *Einfluss der Prozessauslegung auf den Eigenspannungszustand geschliffener Bauteile*, ECG, Aachen, Germany (2003).
31. H. Hamdi, H. Zahouani and J. Bergheau, *J. Mater. Process. Tech.* 147 [3] (2004) 277-285.
32. T.G. Bifano, T.A. Dow and R.O. Scattergood, *J. Manuf. Sci. E-T ASME* 113 [2] (1991) 184-189.
33. R.P. Goehner and M. O. Eatough, *Powder Diffr.* 7 [1] (1992) 2-5.
34. B.D. Cullity, in *Elements of X-ray Diffraction*, Addison-Wesley Publishing Company, Inc. (1978).